

1 **Laser-damage performance of gallium-alloy liquid metal mirrors**

2
3
4 **Gregory S. Demos,^a Brittany N. Hoffman,^a John. C. Lambropoulos,^{a,b} Marcela Mireles^{a,*}**

5 ^aLaboratory for Laser Energetics, University of Rochester, 250 East River Road, Rochester, NY,
6 14623-1299, USA

7 ^bDepartment of Mechanical Engineering, University of Rochester, 275 Hutchison Road,
8 Rochester, NY 14627, USA

9
10 **Abstract.** We explore the characteristics and laser-damage behavior of gallium-based liquid metal
11 alloy mirrors under exposure to ns laser pulses. One of the key advantages of using liquid metal
12 mirrors is the self-healing potential following perturbations arising from exposure to high-power
13 laser pulses. In this work, key performance metrics, such as reflectivity and the laser-damage
14 initiation mechanism and initiation threshold, were investigated using fused-silica cells filled with
15 three different liquid metal Ga alloys. The results suggest that irreversible modification (damage)
16 under 355-nm, 6-ns pulses are associated with the formation of gallium oxide, taking place at a
17 fluence significantly higher than that for damage initiation in conventional metal mirrors. This
18 behavior is believed to arise from the different damage initiation mechanism in liquid metal
19 mirrors requiring increased laser absorbed energy for an irreversible modification of the material
20 surface to occur. This exploratory work is the first of its kind and highlights some favorable
21 performance characteristics of gallium-alloy metal mirrors.

22
23 **Keywords:** liquid metal mirrors, self-healing, laser-induced damage.

24 *Marcela Mireles, E-mail: mmireles@lle.rochester.edu

26 **1 Introduction**

27 High-power laser systems require highly reflective and damage-resistant mirrors to transport and
28 focus the laser light onto the target. Currently, conventional optical components such as multilayer
29 dielectric (MLD) interference coatings are the gold standard; their laser-damage resistance has
30 been improved via advanced coating-deposition techniques and optimized optical designs [1].
31 Metal-coated mirrors, although exhibiting significant energy loss (due to absorption), offer some
32 unique advantages and often are preferred in certain critical locations in laser systems. Specifically,
33 metal-coated mirrors exhibit very broadband reflectivity that is largely uniform over a wide
34 spectral range along with very small sensitivity to the angle of incidence and polarization. In
35 addition, they exhibit low chromatic dispersion and very small wavelength dependence of the
36 reflection phase-shift. Metal-coated mirrors can also work in the infrared spectral region (10 μm
37 and beyond), where MLD mirrors are difficult to manufacture due to the inherent absorptivity of
38 the constituent materials. As a result, metal mirrors represent a viable solution for specific
39 components in various ultrafast laser systems. Another parameter is that fabrication of metal
40 mirrors is far less complicated and thus relatively inexpensive which can be considered as a benefit
41 when used in locations that require frequent replacement of the optic, such as in high contamination
42 regions.

43 A key difference in the damage behavior of metal and MLD mirrors is the damage initiation
44 mechanism. Specifically, the laser-damage performance of metal-coated optics is known to be
45 limited mainly due to the fact that a significant portion of the radiation is absorbed within a thin
46 layer on the surface, increasing their surface temperature to above melting temperature leading to
47 irreversible modification (damage). As a result, the damage threshold is less dependent on the
48 pulse duration [2] contrary to that in MLD optics [1]. Consequently, the difference in the damage

49 threshold between metal-coated and MLD mirror converges as the pulse duration decreases. For
 50 example, recent results from a thin film laser damage competition [3] showed that at 20 fs, 920 nm
 51 excitation, the laser damage threshold of MLD-based mirrors varied between 0.2 J/cm² and 0.9
 52 J/cm² while the damage growth threshold varied between 0.15 J/cm² and 0.4 J/cm². In contrast,
 53 using the same laser and setup, we measured the laser damage initiation and growth thresholds in
 54 gold coated mirrors to be 0.4 J/cm² and 0.6 J/cm², respectively [4]. In comparison, the damage
 55 threshold of gold films reported in [2] is about 0.6 J/cm².

56 It is typically assumed that damage occurs when the surface reaches its melting temperature T_m .
 57 Assuming that there is no heat diffusion during laser irradiation, such as under ultrashort-pulse
 58 excitation, the laser-damage–threshold fluence F_{th} can be found from the energy balance

$$59 \quad \alpha F_{th} = EL_z, \quad (1)$$

60 where α is the absorption coefficient and depends on polarization, angle of incidence, and
 61 wavelength; E is the melting energy; and L_z is the depth of the heated zone. Furthermore, E
 62 encompasses the energy to raise the material to the melting temperature plus the energy required
 63 for the phase transformation and can be expressed as follows

$$64 \quad E = \rho c_p T_m + H_m, \quad (2)$$

65 where H_m is the melting enthalpy, ρ is the mass density, and c_p is the heat capacity.

66 For short pulses, the threshold fluence and the depth of the affected zone are largely
 67 independent of pulse duration. Moreover, to the first-order approximation, the depth of the affected
 68 zone is approximately the absorption length, as previously reported [2]. For long pulses, L_z is
 69 determined by the thermal diffusivity D and the pulse duration τ :

$$70 \quad L_z \approx \sqrt{D\tau}. \quad (3)$$

71 Here we investigate the potential of a paradigm shifting approach: the use of liquid metal
72 mirrors. One of the key advantages of using liquid metal mirrors is their ability to self-heal
73 following perturbations arising from exposure to high-power laser pulses. Considering a liquid
74 metal mirror, it is reasonable to assume that the damage threshold will be associated with the
75 material reaching evaporation conditions. That is, the energy absorbed must be the sum of the
76 energy to reach boiling point plus the evaporation enthalpy. But even in this case, which is related
77 to the ablation threshold of the material, the liquid nature of the metal can facilitate restoration of
78 its initial state following any perturbation on its surface.

79 Among the metals that are in a liquid phase near room temperature, gallium is the only one
80 that is not radioactive (Fr), explosive (Rb, Cs), or toxic (Hg). Despite its metallic classification,
81 gallium displays properties unique amongst most metals due to its peculiar orthorhombic crystal
82 structure in which the distance to the first-nearest neighbor is significantly shorter than to the
83 second-nearest neighbor. The unusual structure favors the formation of discrete diatomic
84 molecules, resulting in weaker intermolecular forces giving rise to its most-distinct physical
85 property—its low melting point of 30°C. The melting point can be further reduced through the
86 creation of alloys with other metals, resulting in metallic materials that can be in a liquid phase
87 even at ambient temperatures and exhibit broadband reflectivity [5,6]. Gallium alloys also exhibit
88 high evaporation temperature ($\sim 2400^\circ\text{C}$) and vaporization enthalpy ($3.7 \times 10^6 \text{ J/kg}$), which,
89 compared to the analogue values for aluminum (melting temperature of $\approx 660^\circ\text{C}$ and melting
90 enthalpy of $\approx 4.0 \times 10^5 \text{ J/kg}$), are indicative that a much higher damage threshold may be expected
91 [see Eq. (2)]. Gallium also exhibits a high thermal conductivity of about 30.2 W/m·K near its
92 melting point (increasing with increasing temperature) [7], thus supporting efficient diffusion of
93 the laser absorbed energy under exposure to longer (nanosecond) pulses.

94 The unique properties of Ga have been explored in various fields including photonic
95 applications. Ga-based liquid reflectors have been developed for telescopes [8,9], demonstrated
96 for laser mode locking [10], stretchable optics [11], optical switching [12], and in an array of liquid
97 metal photonics devices [13,14]. To the best of our knowledge, however, their use for optics
98 suitable for high-power laser systems has not been previously reported.

99 In this work, we investigate the interaction of Ga-based liquid metal mirrors with nanosecond
100 laser pulses including their laser-induced–damage initiation mechanism. The liquid metal mirrors
101 were fabricated by filling polished fused-silica cells with Ga alloys and subsequently testing their
102 reflectance and damage behavior under excitation with 355-nm, 6-ns pulses. The choice of the test
103 laser characteristics is motivated by the need to develop robust optical elements for inertial fusion
104 energy systems [15] which, in some proposed laser driver implementations, will operate in the UV
105 spectral region. The ability of liquid metal mirrors to “self-heal” provides an appealing potential
106 solution. Three different alloys, liquid at room temperature, were used. The results indicate that
107 damage initiation presents as the formation of gallium oxide at a fluence that is evidently higher
108 than that required for damage initiation in conventional solid metal mirrors.

109 **2 Experimental Arrangement**

110 *2.1 Sample Preparation*

111 The selection of Ga alloys for testing was based on their ability to be in liquid phase at room
112 temperature and the availability of materials. High thermal conductivity is anticipated to correlate
113 with higher laser-induced–damage threshold (LIDT). Gallium has a high thermal conductivity
114 [average of ≈ 40.6 W/(m·K) (Ref. 7)], but this value is reduced for Ga alloys, monotonically
115 decreasing as the percentage of Ga decreases. As a result, this change in thermal conductivity may

116 be reflected as a change in the LIDT. In addition, the evaporation temperature and enthalpy may
117 vary between different alloys. Thus, we selected materials with varying percent by mass of gallium
118 due to potential differences in LIDT stemming from the thermal conductivity. We tested the most-
119 commonly utilized Ga alloy, known as “Galinstan” (66.5 Ga/20.5 In/13.0 Sn by weight) along
120 with two GaIn alloys with the following compositions by weight: 75.5 Ga/24.5 In and
121 88.0 Ga/12.0 In. The compositions of the GaIn alloys are, respectively, the eutectic point and the
122 largest Ga percent at which the alloy remains liquid near room temperature. Galinstan was
123 purchased from a vendor, while the GaIn alloys were fabricated in-house via mixing of the metals
124 at $\sim 30^{\circ}\text{C}$.

125 Figure 1 shows a liquid metal mirror fabricated using fused-silica cells having optical-quality
126 surface polishing that were first cleaned with soap, followed by de-ionized water, and then
127 methanol. After drying, the cells were purged with nitrogen to remove moisture and oxygen and
128 then filled with the selected Ga alloys under nitrogen flow. Gallium and its alloys rapidly form a
129 native oxide layer that reduces reflectivity, clearly distinguishable by the naked eye [8]. Nitrogen
130 flow was utilized in an effort to limit the formation of this oxide during the preparation of the
131 samples. The reflectance spectra were measured using a Perkin-Elmer Lambda 900
132 spectrophotometer at a 45° incidence with *s*-polarized light in the 220- to 1100-nm spectral range.

133 Following the collection of reflectance data, the response of Ga alloys to laser damage was
134 investigated, testing with a 355-nm laser and a pulse duration of 6 ns. The LIDT of the material
135 was determined at near-normal incidence ($\sim 7^{\circ}$) for single-shot conditions and for a 10-Hz
136 repetition rate. The damage-initiation behavior was investigated through the determination of the
137 threshold for surface modification using an on-line microscope. The damage sites were further
138 characterized by optical microscopy for a more-detailed analysis of the damage morphology.

139 2.2 Damage-Testing Setup

140 Laser-damage testing was performed using a Quantel Q-smart 450 laser system equipped with
141 second- and third-harmonic crystals, which produces 6 ns nearly Gaussian pulses with an 80-mJ
142 output pulse energy at 355 nm. The schematic of the test setup is shown in Figure 2. The output
143 beam then passed through a waveplate and polarizer, allowing the power reaching the Ga alloy
144 sample to be adjusted, followed by another wave plate, which created *s*-polarized exposure on the
145 sample. Single- or multipulse excitation of the sample was enabled using a programmable shutter
146 and pulse counter. The beam was subsequently directed onto the sample after passing a 1-m
147 focusing lens that created a ~2 mm diameter laser spot at the sample plane. A wedged beam splitter
148 was placed after the focusing lens to produce two auxiliary beams with ~4% of the energy per
149 beam. One beam was directed into an energy meter, allowing the energy of each pulse to be
150 measured, and the second beam was directed into a beam profiler to record the spatial intensity
151 profile of the beam at an equivalent sample plane. An example of the beam profile is shown in
152 Figure 2. The combination of the data from the power meter and beam profiler allowed for *in-situ*
153 calculations of the pulse's peak fluence.

154 A long-working-distance microscope system equipped with a complementary metal-oxide
155 semiconductor (CMOS) camera was used to monitor, *in situ*, the exposure area of the sample's
156 surface during exposure. This laser-damage setup allowed monitoring of the Ga alloys' response
157 to laser pulse exposure over a wide range of fluences using single-pulse and 10-Hz irradiation
158 regimes, providing excellent control over experimental parameters. The R-on-1 testing protocol
159 was used for both single-pulse and 10 Hz irradiation tests with the 10 Hz exposures being 1-minute
160 (600 pulses) in duration for each fluence level tested. "Damage initiation" was defined when any
161 apparent change on the sample's surface was observed using the online microscope system.

162 3 Results

163 Figure 3 shows the measured reflectance of the Ga alloy liquid metal mirror samples at 45°
164 incidence from 220 to 1100 nm for *s*-polarized light. The data were corrected for reflection loss at
165 the air/silica interface. The measured spectra from all three Ga alloys overlap, exhibiting near-
166 identical reflectivity across this wide spectrum. At a 45° incidence, all Ga alloys reach ~88%
167 reflectivity, which agrees with the results reported in Refs. 5 and 6 for the exposed Ga metal. We
168 postulate that a potential experimental artifact due to the use of the cells might be the cause for the
169 decreased reflectivity observed for wavelengths shorter than ~300 nm.

170 Laser-damage testing with 355-nm, 6-ns pulses with nearly Gaussian temporal profile was
171 performed using single-shot and 10-Hz exposures. Despite efforts to minimize oxygen exposure
172 during fabrication via purging with nitrogen, small areas of the surface (as small as ≈ 5 μm in
173 diameter) containing a thin oxide layer were still present and visualized as locations of increased
174 scattering. Consequently, only the areas of the sample that appeared to be oxide-free were
175 subjected to laser-damage testing. The onset of an irreversible material modification, considered
176 as damage, was observed to occur at ~ 0.7 J/cm^2 for 10-Hz laser exposure and was increased to ~ 1
177 J/cm^2 with single-pulse exposure. No significant difference in this behavior was observed between
178 the three alloys tested.

179 Characteristic damage morphologies at the damage-initiation threshold are shown in Figs. 4
180 and 5 for single-pulse and 10-Hz exposure conditions, respectively. In both figures, the images of
181 the sample's surface at the location of beam exposure captured by the on-line microscope (a) prior
182 to exposure and (b) after exposure show the morphology of damage initiation. Figures 4(c) and
183 5(c) show the damage sites on the resulting liquid mirror surface imaged at a higher magnification
184 using an off-line microscope. Figure 5(d) shows the craters created in the fused-silica cell window

185 after removal of the liquid metal and then using a 5% NaOH solution to remove the residual
186 gallium oxide layer as suggested by Borra *et. Al* [8]. Figure 5(e) shows the different depths of the
187 damage craters formed in the window.

188 Features I, II, and III seen in the pre-exposure image in Fig. 5(a) are removed during laser
189 exposure. On the other hand, features 1–7 were generated by the laser exposure and are also
190 observed on the silica window as shown in Fig. 5(d), indicating that damage sites penetrated into
191 the silica window. The depth of those craters varies from sub-100 nm to about 10 μm . Note that
192 this site was exposed to multiple pulses and some of the damage sites were formed earlier. For
193 example, feature 1 was formed after feature 2 under exposure to about the same local peak
194 intensity. The difference in their depth ($\sim 2 \mu\text{m}$ versus $\sim 9 \mu\text{m}$) might be related to the different
195 number of exposure pulses under damage initiation/growth conditions. On the other hand, features
196 3–7 were formed in lower local peak-intensity parts of the beam profile and this might be the
197 reason for the shallower depth. Finally, features 8 and 9 are visible in Fig. 5(c) but not Fig. 5(d),
198 indicative of formation of gallium oxide but not damage to the silica window.

199 Previous work exploring the behavior of gallium under exposure to laser pulses demonstrated
200 the formation of gallium oxide [12,16], which results in significant reduction of the reflectivity
201 due to introduction of non-specular scattering. Our testing was also performed directly on the
202 surface of exposed Galinstan. We observed the formation of oxide in the irradiated area, with an
203 appearance similar to that of the “damage” sites formed in the liquid Ga-alloy mirrors used in this
204 work. These damage sites usually contain bright irregularly-shaped flakes that stay on the liquid
205 surface and can be mechanically swiped away from the damage site. We thus hypothesize that the
206 irreversible material modification observed in the liquid metal mirror samples arises from the

207 formation of gallium oxide. This onset of rapid oxidation is therefore considered the damage-
208 initiation mechanism in liquid Ga alloys contained in silica cells when tested at ambient conditions.

209 The above results indicate that at fluences above threshold, formation of oxide at the interface
210 causes damage to propagate into the fused-silica cell, resulting in formation of pits similar to those
211 formed due to laser damage in silica optics. The exact absorption mechanism is not clear but the
212 significant increase of non-specular reflectance may lead to additional energy deposition and
213 therefore nonlinear increase of the temperature in the damage-site region. The removal of the
214 silicon oxide in the damage crater can provide oxygen for the formation of additional gallium oxide
215 [17], with In acting as a catalyzer increasing the rate of oxidation [18]. Note, for example, the size
216 difference of feature 4 as it appears in Figs. 5(c) and 5(d)—specifically the diameter of feature 4
217 is much larger in Fig. 5(c) than in Fig. 5(d), indicative of that the area of oxide formation extends
218 well beyond the area of crater formation. The difference in size was also observed for all other
219 features including 3 to 6 as well as 9.

220 To understand the origin of the difference in the oxide induced LIDT under single pulse and
221 10-Hz exposure ($\sim 1 \text{ J/cm}^2$ and $\sim 0.7 \text{ J/cm}^2$, respectively), 1D modeling of heat transfer in a semi-
222 infinite medium was performed using the formalism presented in Ref. 19. The temperature T as a
223 function of depth z inside the gallium liquid layer and time t assuming a surface heat flux
224 $\dot{q}_s (\text{W/m}^2)$ from the absorbed laser energy can be expressed as:

$$225 \quad T(z, t) - T_i = \frac{\dot{q}_s}{k} \left[\sqrt{\frac{4\alpha t}{\pi}} \exp\left(-\frac{z^2}{4\alpha t}\right) - \text{zerfc}\left(\frac{z}{2\sqrt{\alpha t}}\right) \right],$$

226
227 where k is the thermal conductivity, α is the thermal diffusivity, t is the time, and z is the
228 distance into the surface. These material parameters for Galinstan and gallium are, respectively,

229 1300/2400°C boiling point, 16.5/40.6 W/m.K thermal conductivity, 296/ 371 J/(kg·K) heat
230 capacity, and 6.44/5.91g/cm³ density. These parameters change with temperature⁴ and thus, this
231 estimation only enables comparison. We also do not consider the heat conduction toward the silica
232 cell window due to its relatively very low value. The estimated absorbed energy required to reach
233 near-evaporation temperature (assuming initial room temperature of 22 °C) from a 10-ns, flat in
234 time, pulse in Galinstan and gallium is 0.11 J/cm² and 0.20 J/cm², respectively. These correspond
235 to a laser fluence at normal incidence (based on a measured reflectance of ≈85%) of 0.73 J/cm²
236 and 1.3 J/cm² for Galinstan and gallium, respectively. These values are similar to those obtained
237 during our laser-damage testing.

238 The analytical result above also can be used to derive a Figure of Merit to compare the mirror
239 performance of different materials. Assuming the same pulse duration, the FOM is:

$$240 \quad \text{FOM} = \Delta T (k \rho c_p)^{1/2}$$

241 For Ga, the FOM is 2300 J/(cm² s^{1/2}), while for Al it is 1400 J/(cm² s^{1/2}), primarily due to its
242 low melting point (660 °C) despite its higher thermal conductivity. It is clear, therefore, that Ga is
243 expected to withstand a much higher “damage threshold” fluence than Al. Also notice that the
244 thermal conductivity for Al may well be reduced due to any defects during evaporation of the
245 mirror coating. Furthermore, eq. 3 denotes that the high thermal diffusivity of Al causes the melted
246 layer in Al to be more than twice as thick as the Ga evaporated layer.

247 Figure 6(a) depicts in logarithmic scale the 1D modeling results of temperature as a function
248 of time on the surface of gallium as well as 0.5 μm and 1 μm below the surface under exposure to
249 a single 10-ns, flat in time laser pulse with a fluence of ≈1.3 J/cm². The energy deposited allows
250 the surface to reach a value near boiling temperature by the end of the laser pulse and subsequently

251 rapidly decreases. The peak temperatures below the surface are significantly lower, depending on
252 the specific depth while the overall peak temperature is highly localized near the surface.

253 For the case of 10-Hz operation with a second pulse arriving at $t = 0.1$ s, however, the surface
254 temperature does not return to its original value. As a result, continuous exposure to laser pulses
255 at 10 Hz will lead to accumulation of heat. Consequently, operation at 10 Hz will lead to a higher
256 local temperature than when using single-pulse exposure. Therefore, assuming that there is a
257 specific temperature that initiates the formation of oxide, the required fluence will be lower when
258 exposure is at 10 Hz compared to a single pulse. This explains the lower value of LIDT at 10 Hz
259 compared to the single pulse. It also supports the hypothesis that a specific temperature is required
260 for the rapid and irreversible formation of oxide on the surface.

261 Figure 6(a) displays in linear scale the temperature on the surface for the case of gallium and
262 aluminum under same excitation condition (as in Fig. 5a) highlighting the ability of gallium to
263 absorb more laser energy before reaching its boiling point compared to that for aluminum for
264 reaching its melting point. One may also need to consider the enthalpy of vaporization (3700 J/g)
265 for gallium compared to the enthalpy of fusion (3.76 J/g) in aluminum for a more accurate estimate.
266 To further elucidate this point, damage testing of a protected aluminum mirror obtained from a
267 leading supplier was performed using the same experimental configuration and test system used
268 in the study of the Ga-based liquid metal mirrors. The damage threshold of the protected aluminum
269 mirror was found to be about 0.35 J/cm^2 and 0.42 J/cm^2 under single pulse and 10-Hz exposure,
270 respectively.

271 **4 Discussion**

272 The laser-induced damage in liquid metal mirrors made from gallium alloys contained in silica
273 cells at ambient conditions manifested through the localized formation of gallium oxide at the peak

274 fluence of the laser exposure sites, which grows in area under additional exposure and is not
275 reversible. The on-line microscope system detected microscopic modifications, which may be
276 related to oxide formation from laser exposure at lower fluences, but these modifications dissolved
277 under subsequent exposure to laser pulses and did not impact the reflectivity of the sample. Since
278 the formation of oxide occurs naturally in Ga-based materials, the deposition of heat through rising
279 fluence favors this reaction and thus increases the rate of oxide formation in areas exposed to high
280 fluence. This increase in the rate of oxidation with increasing temperature is known to occur in
281 various metal materials. While the formation of oxide is expected in Ga alloys exposed to ambient
282 conditions, the oxide observed to form at the interface between the fused silica and the liquid metal
283 may be rather surprising due to lack of direct exposure to oxygen. It is possible that Ga may be
284 reacting with oxygen from the fused-silica cell, with oxygen dissolved within the liquid metal, or
285 with oxygen at the interface between the cell and the metal. Therefore, the use of a silicon oxide
286 cell filled in a nitrogen-rich environment may compromise the LIDT.

287 The management of oxide formation is crucial for successful Ga-based liquid metal optics.
288 Native oxide formation diminishes the reflectivity of the sample, along with making the material
289 more vulnerable to laser-induced damage. There are numerous options for controlling this oxide
290 layer, with implementation in a vacuum or nitrogen environment lacking oxygen likely to
291 significantly reduce, if not entirely eliminate, the formation of oxide. As for windows covering the
292 liquid metal, a non-oxide window may be preferred.

293 Although the damage threshold of the various Ga alloys can be further increased with
294 optimization of our methodology, it must be noted that the results of this work demonstrated that
295 the liquid metal alloys display a higher LIDT than conventional metal mirrors. For example, the
296 LIDT of Ga-based alloy liquid metal mirror was found to be about twofold higher compared to

297 that of a conventional protected aluminum mirror (0.7 J/cm^2 vs 0.35 J/cm^2 for 10-Hz exposure and
298 1 J/cm^2 vs 0.42 J/cm^2 for single pulse exposure). Further studies in an oxygen-controlled
299 environment will enable the study of the fundamental limit of damage due to ablation (evaporation,
300 shock generation, etc.) rather than via an intermediate step due to oxide formation, which is the
301 limit observed in this work.

302 For UV laser applications, such as for optical components for the laser drivers in inertial
303 confinement power systems [15], aluminum is the best choice among the currently used metal
304 coating materials owing to its optical constants that provide extended reflectivity down to the 100
305 nm spectral range [20, 21]. The results shown in Figure 3 demonstrate that liquid metal Ga-based
306 alloys also exhibit such extended reflectivity in the UV spectral range. Bieri *et al.* proposed [22]
307 that the final beam pointing mirror in laser fusion energy power plants, which will be exposed to
308 a variety of damage threats, be based on grazing incidence metal mirrors (GIMMs). Moir *et al.*
309 later proposed, based on modeling considerations, the use of Grazing Incidence Liquid Metal
310 Mirrors (GILMM) as robust final optics [23]. The results presented in this work are suggestive that
311 Ga-based metal mirrors maybe an approach that should be considered. However, investigation of
312 this concept is outside of the focus of this work.

313 **Conclusion**

314 This work represents an exploratory study of the potential strengths and limitations of gallium-
315 based liquid metal mirrors for use in high power laser systems. Although no specific application
316 was considered in depth at this present time, the results suggest that, compared to conventional
317 thin metal film optics, liquid metals can provide a higher damage threshold in certain arrangements
318 over a wide spectral range extending into the UV spectral region. Another appealing property of
319 liquid metal mirrors is related to their ability to “self-heal” after an ablation (damage) event without

320 producing absorbing species, such as sub-stoichiometric oxides typically observed in dielectric
321 materials, that can facilitate additional damage (damage growth) under exposure to subsequent
322 laser pulses. The main limitation observed in this study, which was performed at ambient
323 conditions, is the formation of oxide at the location of laser exposure, which has been defined as
324 the damage initiation mechanism. Future work is needed to determine the potential of Ga-based
325 liquid metal mirrors to address currently unmet needs for specific applications such an alternative
326 solution for damage-sensitive optics in short pulse laser systems or for inertial fusion energy laser
327 drivers.

328 *Disclosures*

329 The authors declare no conflicts of interest.

330 *Code, Data, and Materials Availability*

331 Raw imaging data underlying the results presented in this paper are not publicly available at this
332 time but may be obtained from authors upon request. Biographies of the authors are not available
333 in this manuscript.

334 *Acknowledgments*

335 This material is based upon work supported by the Department of Energy [National Nuclear
336 Security Administration] University of Rochester “National Inertial Confinement Program” under
337 Award Number(s) DE-NA0004144.

338 This report was prepared as an account of work sponsored by an agency of the United States
339 Government. Neither the United States Government nor any agency thereof, nor any of their
340 employees, makes any warranty, express or implied, or assumes any legal liability or responsibility

341 for the accuracy, completeness, or usefulness of any information, apparatus, product, or process
342 disclosed, or represents that its use would not infringe privately owned rights. Reference herein to
343 any specific commercial product, process, or service by trade name, trademark, manufacturer, or
344 otherwise does not necessarily constitute or imply its endorsement, recommendation, or favoring
345 by the United States Government or any agency thereof. The views and opinions of authors
346 expressed herein do not necessarily state or reflect those of the United States Government or any
347 agency thereof.”

348

349
350
351
352
353
354
355
356
357
358
359
360
361
362
363
364
365
366
367
368
369
370
371
372

References

1. C. J. Stolz and R. A. Negres, “Ten-year summary of the Boulder Damage Symposium annual thin film laser damage competition,” *Opt. Eng.*, 57, 121910, (2018).
2. Stuart, B. C., Feit, M. D., Herman, S., Rubenchik, A. M., Shore, B. W. and Perry, M. D., “Optical ablation by high-power short-pulse lasers,” *J. Opt. Soc. Am. B* 13(2), 459-468 (1996).
3. R. A. Negres, K. R. P. Kafka, C. Smith, M. Stehlik, S. Olandt, S. G. Demos and A. Rigatti “Broadband, 920-nm mirror thin film damage competition”, *Proc. of SPIE Vol. 12726*, 1272606 (2023)
4. K. R. P. Kafka et. Al., manuscript in preparation.
5. Akashev, L. A. and Kononenko, V. I., “Optical properties of liquid gallium-indium alloy,” *Tech. Phys.* 43(7), 853–854 (1998).
6. Gutiérrez, Y., Losurdo, M., García-Fernández, P., Sainz de la Maza, M., González, F., Brown, A. S., Everitt, H. O., Junquera, J. and Moreno, F., “Dielectric function and plasmonic behavior of Ga(II) and Ga(III),” *Opt. Mat. Express* 9(10), 4050–4060 (2019).
7. Prokhorenko, V. Ya., Roshchupkin, V. V., Pokrasin, M. A., Prokhorenko, S. V. and Kotov, V. V., “Liquid gallium: Potential uses as a heat-transfer agent,” *High Temp.* 38(6), 954–968 (2000).
8. Borra, E. F., Tremblay, G., Huot, Y. and Gauvin, J., “Gallium liquid mirrors: Basic technology, optical-shop tests and observations,” *Publ. Astron. Soc. Pac.* 109(733), 319–325 (1997).
9. A. E. Potter and M. Mulrooney, “Liquid metal mirror for optical measurements of orbital debris”, *Adv. Space Res.* 19, 213-219 (1997)
10. P. Petropoulos, D. J. Richardson, S. Dhanjal, and N. I. Zheludev, “Passive Q-switching of fiber lasers using a broadband liquefying gallium mirror”, *Appl. Phys. Lett.* 74, 3619 (1999)
11. M. G. Mohammed, M. D. Dickey, “Strain-controlled diffraction of light from stretchable liquid metal micro-components”, *Sens. Actuator A Phys.* 193, 246-250 (2013)

- 373 12. V. Albanis, S. Dhanjal, V. A. Fedotov, K. F. MacDonald, and N. I. Zheludev, P. Petropoulos, D.
374 J. Richardson, V. I. Emel'yanov, "Nanosecond dynamics of a gallium mirror's light-induced
375 reflectivity change", Phys. Rev. B 63, 165207 (2001)
- 376 13. X. Wu, H. Fang, X. Ma and S. Yan, "Gallium-Based Liquid Metals: Optical Properties,
377 Applications, and Challenges", Adv. Optical Mater., 2301180 (2023)
- 378 14. P. Q. Liu, X. Miao, S. Datta, "Recent advances in liquid metal photonics: technologies and
379 applications", Opt. Mat. Express 13, 699 (2023)
- 380 15. H. Abu-Shawareb et al., "Lawson Criterion for Ignition Exceeded in an Inertial Fusion
381 Experiment", Phys. Rev. Lett **129**, 075001 (2022)
- 382 16. N. M. Bulgakova A. N. Panchenko, "Formation of microtower structures on nanosecond laser
383 ablation of liquid metals" Appl Phys A 98, 393–400 (2010)
- 384 17. Cochran, C. N., and L. M. Foster, "Vapor pressure of gallium, stability of gallium suboxide
385 vapor, and equilibria of some reactions producing gallium suboxide vapor" J. Electrochem. Soc.
386 109.2 (1962) 144
- 387 18. Vogt, Patrick, et al., "Metal-exchange catalysis in the growth of sesquioxides: Towards
388 heterostructures of transparent oxide semiconductors." Phys. Rev. Lett. 119.19 (2017): 196001
- 389 19. M. Mireles, B. Hoffman, S. MacNally, S. Lakshmanan, J. Lambropoulos, A. Rigatti, and S. G
390 Demos "Direct-write laser assisted patterning of form birefringence in waveplates fabricated by
391 glancing angle deposition", Optica 10, 657 (2023).
- 392 20. *Handbook of Optical Constants of Solids*. Edward D. Palik, ed. (1985). Academic Press.
- 393 21. *Handbook of Optical Constants of Solids II*. Edward D. Palik, ed. (1991). Academic Press.
- 394 22. R. L. Bieri M. W. Guinan "Grazing Incidence Metal Mirrors as the Final Elements in a Laser
395 Driver for Inertial Confinement Fusion," Fusion Technol.,19, 673 (1991)
- 396 23. R. W. Moir, "Grazing Incidence Liquid Metal Mirrors (GILMM) for Radiation Hardened Final
397 Optics for Laser Inertial Fusion Energy Power Plants," Fusion Eng. Des., 51–52, 1121 (2000)
- 398

399 **Caption List**

400 **Figure 1:** (a) Liquid metal mirrors were fabricated using fused-silica cells that were filled with the
401 Ga alloy. The mirror surface is outlined in red. (b) The samples were then mounted on a holder to
402 perform laser-exposure experiments.

403 **Figure 2:** A schematic of the laser-exposure setup and the laser beam profile taken at an equivalent
404 plane to the sample. BS: Beam splitter; L: Lens; POL: Polarizer; WP: Waveplate; EM: Energy
405 meter; BP: Beam profiler; CM: Camera; WL: White light illuminator.

406 **Figure 3:** Reflectance spectra for the three Ga alloys: Galinstan (66.5 Ga/20.5 In/13.0 Sn wt%) and
407 GaIn alloys with varying percent by mass of indium: 75.5 Ga/24.5 In and 88.0 Ga/12.0 In.

408 **Figure 4:** Single-pulse exposure: (a) on-line microscope image of a Ga alloy liquid mirror prior to
409 and (b) following laser exposure at about 1 J/cm². (c) Off-line higher magnification image of the
410 same damage site.

411 **Figure 5:** Ten-Hz exposure: (a) on-line microscope image of a Ga alloy liquid mirror prior to and
412 (b) following laser exposure at about 0.7 J/cm². (c) Off-line higher magnification images of the
413 damage site on the resulting liquid mirror surface. (d) Image obtained on the optical profilometer
414 after removal of the Ga alloy showing the formation of craters in the fused-silica cell window. (e)
415 Depth profiles of the craters along lines indicated in (d).

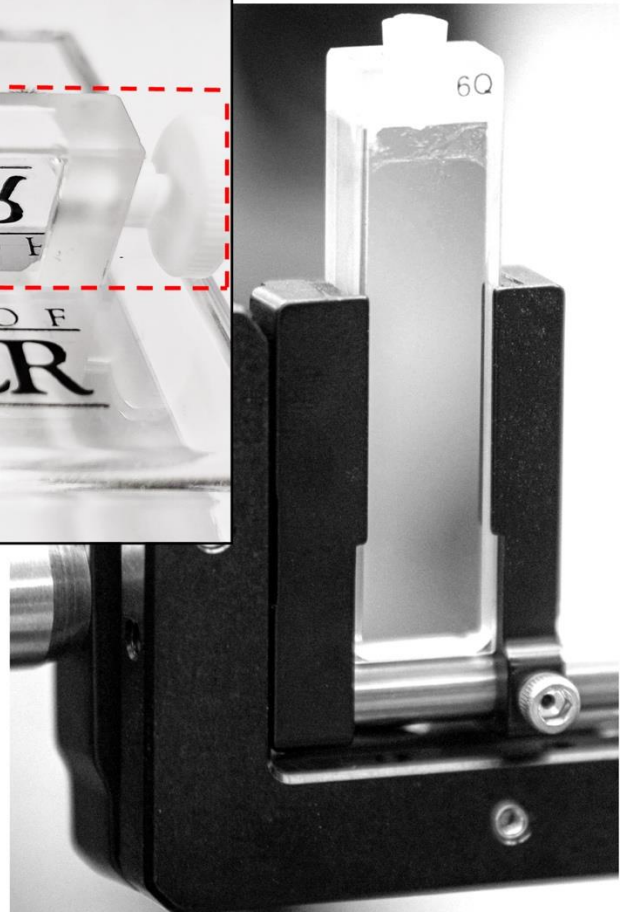
416 **Figure 6:** One-dimensional modeling of the temperature at the surface of gallium as well as 0.5
417 μm and 1 μm below the surface of gallium under exposure to a single 10-ns, flat in time laser pulse
418 with a fluence of 1.3 J/cm² as a function of time in logarithmic scale (a). The temperature at the
419 surface in gallium and aluminum in linear scale under same laser excitation conditions (b). For
420 both plots $t = 0$ is defined at the onset of the pulse.

421

422 Figure 1



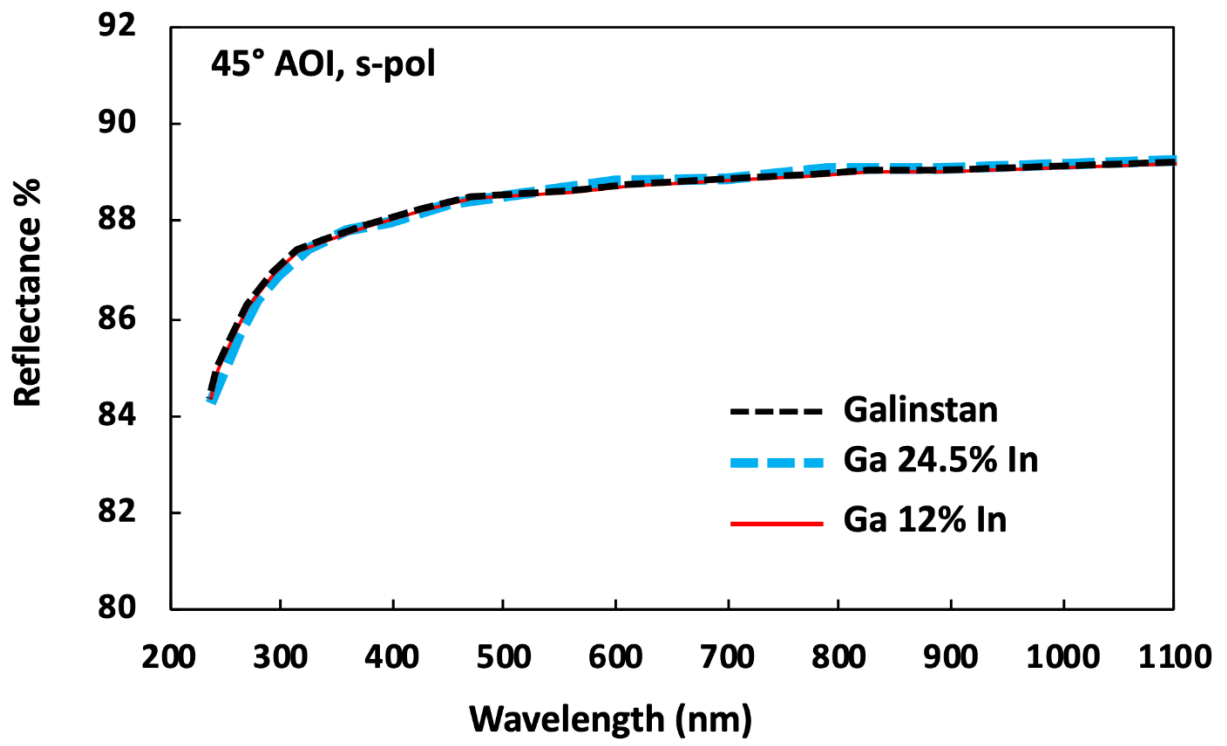
(a)



(b)

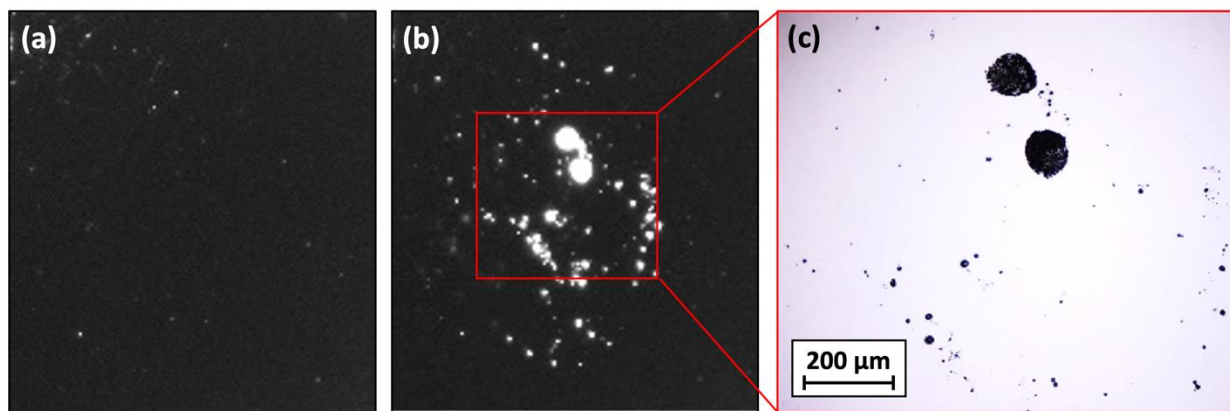
423
424

428 Figure 3



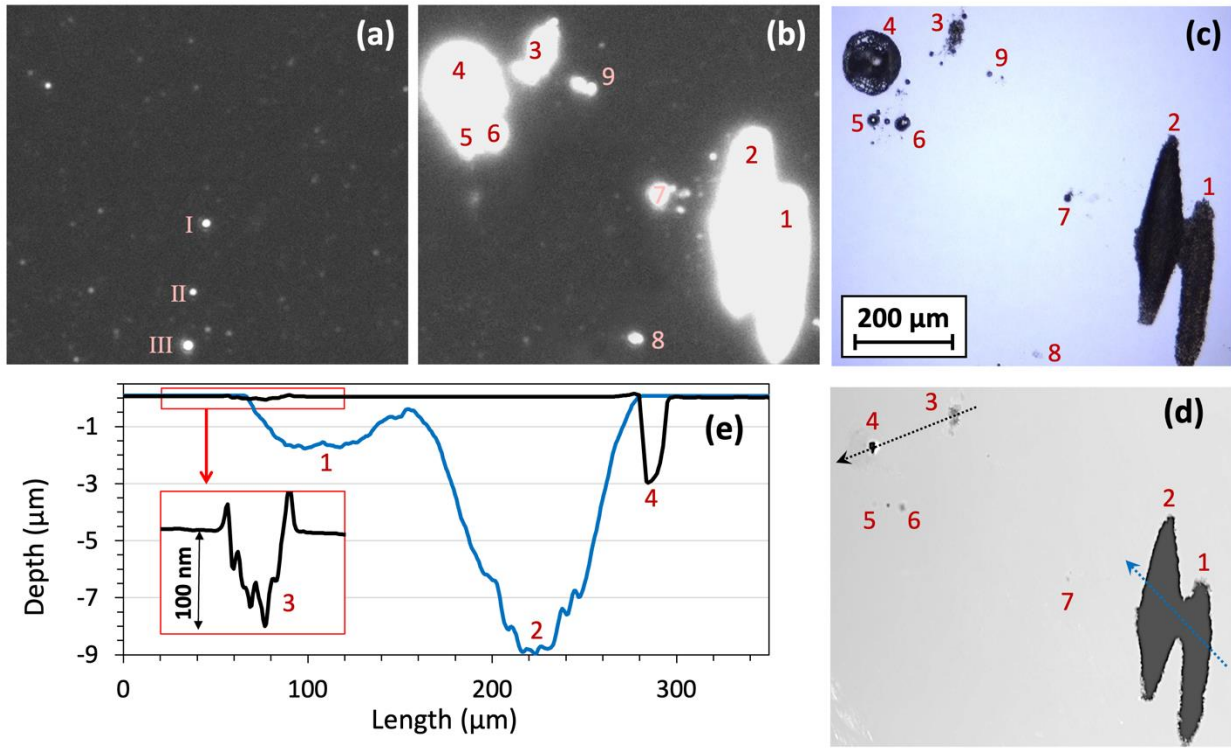
429
430

431 Figure 4



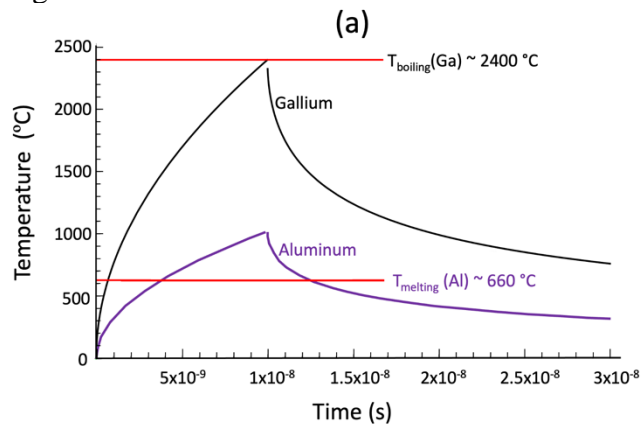
432
433

434 Figure 5



435
436

437 Figure 6



438

